*Article*

# A Proteomic Study on the Personalized Protein Corona of Liposomes. Relevance for Early Diagnosis of Pancreatic DUCTAL Adenocarcinoma and Biomarker Detection

Luca Digiacomo [1], Francesca Giulimondi [1], Daniela Pozzi [1], Alessandro Coppola [2], Vincenzo La Vaccara [2], Damiano Caputo [2] and Giulio Caracciolo [1,*]

[1] Nanodelivery Lab, Department of Molecular Medicine, Sapienza University of Rome, 00161 Rome, Italy; luca.digiacomo@uniroma1.it (L.D.); francesca.giulimondi@uniroma1.it (F.G.); daniela.pozzi@uniroma1.it (D.P.)
[2] General Surgery Unit, University Campus Bio-Medico di Roma, 00128 Rome, Italy; a.coppola@unicampus.it (A.C.); v.lavaccara@unicampus.it (V.L.V.); d.caputo@unicampus.it (D.C.)
* Correspondence: giulio.caracciolo@uniroma1.it

**Abstract:** Due to late diagnosis, high incidence of metastasis, and poor survival rate, pancreatic cancer is one of the most leading cause of cancer-related death. Although manifold recent efforts have been done to achieve an early diagnosis of pancreatic cancer, CA-19.9 is currently the unique biomarker that is adopted for the detection, despite its limits in terms of sensitivity and specificity. To identify potential protein biomarkers for pancreatic ductal adenocarcinoma (PDAC), we used three model liposomes as nanoplatforms that accumulate proteins from human plasma and studied the composition of this biomolecular layer, which is known as protein corona. Indeed, plasma proteins adsorb on nanoparticle surface according to their abundance and affinity to the employed nanomaterial, thus even small differences between healthy and PDAC protein expression levels can be, in principle, detected. By mass spectrometry experiments, we quantified such differences and identified possible biomarkers for PDAC. Some of them are already known to exhibit different expressions in PDAC proteomes, whereas the role of other relevant proteins is still not clear. Therefore, we predict that the employment of nanomaterials and their protein corona may represent a useful tool to amplify the detection sensitivity of cancer biomarkers, which may be used for the early diagnosis of PDAC, with clinical implication for the subsequent therapy in the context of personalized medicine.

**Keywords:** pancreatic cancer; early detection; cancer biomarkers; biomolecular corona

## 1. Introduction

Nanotechnologies represent an emerging science that has been recognized as a potential game-changer in cancer management [1]. When Nanoparticles (NPs) interact with biological fluids (e.g., plasma, urine), they are coated with a layer of molecules, which is called biomolecular corona (BC), that provide NPs with a totally new biological identity [2]. Since the BC is mainly made up of proteins, it is often referred to as the protein corona (PC). The characteristics (e.g., shape, composition, electric charge, etc.) [3] of the PC depend on different factors. Some of these are related to the source with which NPs interact and to the environmental and experimental conditions (e.g., pH, temperature, type of biological fluid, etc.), [4] others depend on the type of used NPs (e.g., liposomes, gold, etc.) and on their chemical-physical characteristics (e.g., shape, size, electric charge, etc.) [5]. These peculiarities also allowed to demonstrate that the PC adsorbed to the surface of NPs is not only specific to different oncological pathologies but is also personalized from subject to subject [6–8].

These abilities have been proved to be very useful in the development of diagnostic tools [9–11] that are able to detect, with high sensitivity and specificity, insidious and highly lethal tumor such as pancreatic cancer [12]. Pancreatic adenocarcinoma is burdened by a

poor prognosis in the majority of cases. Indeed, usually asymptomatic in its early stages and having a very aggressive biological behavior, it is often diagnosed in an advanced stage to be treated effectively [13]. Nevertheless, recent advances in the field of pancreatic adenocarcinoma early detection allowed to demonstrate how NPs can be effectively used for early diagnosis of this lethal disease. Furthermore, since in addition to the diagnostic ability [14] the analysis of the PC also proved to be useful in distinguishing among pancreatic cancers in different stages of disease [15], it is possible to hypothesize the use of nanotechnologies in the "molecular" staging of pancreatic cancer. Moreover, taking into account that proteins alterations represent the hallmark of carcinogenesis and that the analysis of the protein corona obtained using nanoparticle enabled blood test are promising in pancreatic cancer detection, deeper analysis of the protein pattern forming the PC could lead to the identification of novel biomarkers useful in pancreatic cancer early detection.

## 2. Materials and Methods

### 2.1. Preparation of Liposomes

In this work we used Cholesterol (Chol), DOPC (dioleoylphosphatidylcholine), DOPE (dioleoylphosphatidylethanolamine), DOPG (1,2-dioleoylsn-glycero-3-phospho-(10-rac-glycerol)), and DOTAP (1,2-dioleoyl-3-trimethylammonium-propane) to prepare liposomes by thin-film hydration method. Chol was purchased from Sigma Aldrich (St. Louis, MO, USA), all the other lipids were purchased from Avanti Polar Lipids (Alabaster, AL, USA). Three types of liposomes were prepared from DOPG, DOPC-Chol (1:1 molar ratio), and DOTAP–DOPE (1:1 molar ratio) and are hereafter referred to as $L_1$ (anionic), $L_2$ (neutral) and $L_3$ (cationic), respectively. After dissolving the lipid mixtures in chloroform, letting the solvent evaporate under vacuum for 2 h, lipid films were hydrated with phosphate saline buffer (PBS) to a final concentration of 1 mg/mL. Finally, liposomes were extruded through a 100 nm polycarbonate carbonate filter by employing an Avanti Mini-Extruder (Avanti Polar Lipids, Alabaster, AL, USA).

### 2.2. Human Plasma Collection and Protein Corona Formation

Human blood (HP) was collected from healthy donors and patients diagnosed with pancreatic ductal adenocarcinoma (PDAC). The study was approved by the Ethical Committee of University Campus Bio-Medico di Roma. Plasma was obtained from blood by centrifugation at $1000\times g$ for 5 min. Biocoronated formulations were obtained by incubating liposomes with HP (1:1 $v/v$) for 1 h at 37 °C.

### 2.3. Size and Zeta Potential Measurements

All size and zeta-potential measurements were carried out at room temperature using a Zetasizer Nano ZS90 system (Malvern, UK), operating under non-invasive back scattering configuration. For both size and zeta potential, 10 μL of each sample were diluted with 990 μL of distilled water. Results are given as mean ± standard deviation of three measurements. Experiments were performed on unwashed samples. Consequently, contamination from biological nanoparticles was not examined and could not be excluded. However, previous studies indicated that it should produce minor, if any, effect on the size of liposome-protein complexes [16,17].

### 2.4. Protein Corona Composition

Liposome-HP samples were pelleted at g for 15 min at 4 °C, then washed three times with PBS. After washing three times with 10 mmol/L Tris HCl (pH 7.4), 150 mmol/L NaCl, and 1 mmol/L EDTA, the pellet was air-dried and resuspended in 40 mL of 8 mol/L urea, and 50 mmol/L $NH_4HCO_3$ (pH = 7.8). The obtained protein solution was reduced with 2 mL of 200 mmol/L DTT, alkylated with 8 mL of 200 mmol/L IAA and added with 8 mL of 200 mmol/L DTT. Finally, the solution was diluted with 50 mmol/L $NH_4HCO_3$ and digested overnight with 2 mg of trypsin at 37 °C. Digested peptides were desalted using the SPE C18 column and analyzed by nano-high-performance liquid chromatography (HPLC)

coupled to tandem mass spectrometry, by means of a Dionex Ultimate 3000 system (Dionex Corporation, Sunnyvale, CA, USA) directly connected to a hybrid linear ion trap-Orbitrap mass spectrometer (Orbitrap LTQ-XL, Thermo Scientific, Bremen, Germany) provided with a nanoelectrospray ion source. Reversed-phase (RP) chromatography was employed to separate the peptide mixtures, with a 3 h optimized LC gradient composed of mobile phase of ddH$_2$O/HCOOH (99.9/0.1, *v/v*) and mobile phase of ACN/HCOOH (99.9/0.1, *v/v*). MS spectra of eluting peptides were collected over an m/z range of 350–1700, RAW data were submitted to Mascot (v1.3, Matrix Science, London, UK) and finally compared to the non-redundant Swiss-Prot database (09-2014, 546,000 sequences, Homo Sapiens taxonomy restriction). Validation of peptide identifications were approved if the probability threshold set by the PeptideproPhet algorithm was higher than 95%, protein identifications were accepted only for probability >99.0% and if they contained at least two unique peptides. Further details of the employed technique can be found elsewhere [7]. Results are provided as average ± standard deviation of three independent replicates.

### 2.5. Statistical Analysis

Data analysis and the corresponding graphs were performed using custom Matlab (Mathwork) scripts.

### 3. Results

In this work, we carried out a comparative analysis of the BC formed on three liposomal formulations upon incubation with human plasma from non-oncological (CTR) and pancreatic cancer (PDAC) patients. Size and Zeta potential of the employed liposomes were measured by dynamic light scattering and electrophoretic light scattering, respectively (Table 1). By this preliminary analysis, we found that all the formulations had homogenous size distributions, with average hydrodynamic diameter ranging between 140 nm and 180 nm and polydispersity index smaller than 0.2. Furthermore, due to their different lipid compositions, the corresponding zeta potentials were negative, almost neutral and positive for L$_1$, L$_2$ and L$_3$, respectively. After exposure to human plasma, we detected a remarkable increase of size and polydispersity for all the liposome-plasma dispersions and the measured values of zeta potential ranged within about −30 mV and −40 mV, independently on the original surface charge of the bare liposomes (Table 1). This experimental evidence is in agreement with the expected behavior of NPs in biological media. Indeed, the adsorption of plasma proteins is generally responsible for an increase of the hydrodynamic diameter (possibly leading to particle aggregation), a reduction of the dispersion's homogeneity and a "normalization" of the surface zeta potential to common negative plateau-values.

By incubating the employed liposomal formulations (anionic, neutral and cationic) with human plasma from *n* = 3 healthy donors and *n* = 3 pancreatic cancer patients, we obtained a set of 18 independent coronas, which were subdivided into six classes, according to the scheme of Figure 1A. The corresponding protein corona compositions were assessed by nano-liquid chromatography-mass spectrometry. This allowed us to measure the relative abundance of the detected proteins in each of the investigated samples. Figure 1B shows the Venn diagrams depicting the number of identified proteins in control (light colors) and pancreatic cancer (dark colors) coronas for L$_1$, L$_2$, and L$_3$ (from top to bottom, respectively). Interestingly, the anionic formulation recruited a larger number of different proteins with respect to the other ones and, for all the liposomes, unique corona proteins on CTR and PDAC samples were detected. These preliminary outcomes point out that (i) the lipid composition of the employed formulations affects the resulting protein corona and (ii) the protein corona may reveal significant changes of certain plasma levels, which are specifically due to the pathological condition. Whilst, to date, these aspects are not surprising, here, we try to give a deeper insight by a comparative analysis. First, we studied the global effects of the NP's lipid content on the resulting corona composition.

**Table 1.** Zeta potential, size and polydispersity index of bare liposomes and their counterparts after exposure to human plasma from healthy donors and pancreatic ductal adenocarcinoma (PDAC) patients.
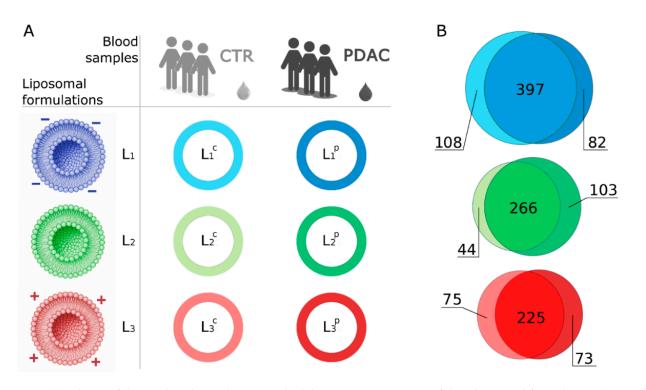
| Bare Liposomes | Zeta Potential (mV) | Size (nm) | PdI |
|---|---|---|---|
| L1 | $-69.1 \pm 4.5$ | $146 \pm 3$ | $0.113 \pm 0.076$ |
| L2 | $-3.5 \pm 1.2$ | $173 \pm 3$ | $0.050 \pm 0.001$ |
| L3 | $46.5 \pm 2.3$ | $154 \pm 11$ | $0.170 \pm 0.040$ |
| **Liposome + Healthy Plasma** | **Zeta Potential (mV)** | **Size (nm)** | **PdI** |
| L1 | $-42.7 \pm 1.3$ | $179 \pm 3$ | $0.406 \pm 0.052$ |
| L2 | $-28.4 \pm 2.3$ | $251 \pm 8$ | $0.378 \pm 0.038$ |
| L3 | $-38.1 \pm 1.1$ | $233 \pm 4$ | $0.330 \pm 0.090$ |
| **Liposome + PDAC Plasma** | **Zeta Potential (mV)** | **Size (nm)** | **PdI** |
| L1 | $-35.6 \pm 0.7$ | $205 \pm 4$ | $0.262 \pm 0.066$ |
| L2 | $-31.3 \pm 2.1$ | $269 \pm 3$ | $0.270 \pm 0.068$ |
| L3 | $-28.3 \pm 1.3$ | $240 \pm 4$ | $0.350 \pm 0.020$ |



**Figure 1.** (**A**) Scheme of the employed samples: we studied the corona composition of three liposomal formulations (L1, L2, and L3) with different surface charge (anionic, neutral and cationic, respectively), upon incubation with human plasma from non-oncological (CTR) and pancreatic cancer (PDAC) patients. (**B**) Venn diagrams depicting the number of detected proteins in CTR and PDAC coronas for each liposomal formulation.

As the main differences among the physical-chemical properties of the employed formulations are related to their surface charge, we focused on the distributions of isoelectric points (pI) of the adsorbed proteins. As shown in Figure 2, the coronas formed on the anionic liposome had a larger portion of high-pI proteins, with respect to the neutral and cationic systems. Indeed, the cumulative abundance of proteins with pI > 8.5 was about three times higher on $L_1$ than $L_3$ (Table 2). Conversely, we found an opposite trend for low-pI proteins (pI < 6), whose abundance reached about 50% of the whole corona for the cationic liposome, versus 41% and 42% for the anionic and neutral counterparts, respectively. Finally, the dominant portion of the pI distributions for the neutral system ($L_2$) was the range of intermediate isoelectric points (6 < pI < 8.5). These outcomes are in

agreement with the expectations and elucidate the crucial role of NP's surface charge on the protein corona formation. Indeed, the isoelectric point of a molecule is the pH at which that molecule carries no net electrical charge. Depending on the solution pH, a protein can act as an anionic, neutral or cationic object. If the solution pH is above the pI of a generic protein, that protein's surface is negatively charged. Likewise, at a solution pH that is below the pI, the protein surface is predominantly positively charged. By considering that the pH of human plasma is about 7.4, proteins with low pI are negatively charged objects and tend to be attracted to cationic particles. Proteins with high pI preferentially adsorb on anionic surfaces and proteins with intermediate pI act mainly as neutral systems. We finally point out that despite the electrostatic interaction is not the only one driving the protein adsorption on nanomaterials, our results suggest that it has a great impact on shaping the overall composition of the corona. Thus, detailed knowledge of the role of NP's surface charge may be employed to modulate properly the interactions in biological environments for biomedical purposes (e.g., discovery of biomarkers for cancers, diagnosis by nanomaterials' corona and smart targeting for drug delivery applications).
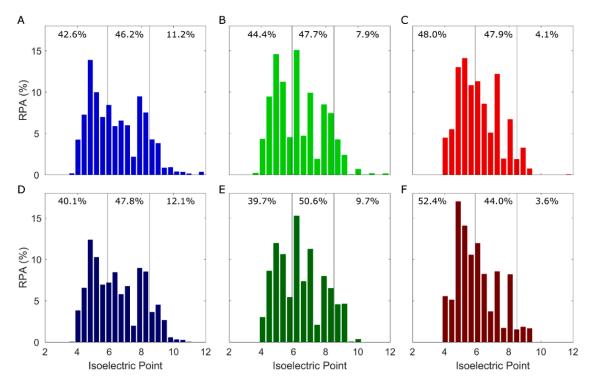


**Figure 2.** Isoelectric point distributions of the detected corona proteins on (**A**–**C**) healthy and (**D**–**F**) PDAC coronas for (**A**,**D**) $L_1$, (**B**,**E**) $L_2$ and (**C**,**F**) $L_3$.

**Table 2.** Cumulative abundances of corona proteins with low (pI < 6), intermediate (6 < pI < 8.5) and high (pI > 8.5) isoelectric points for L1, L2, and L3. Values are reported as averages over healthy and PDAC coronas.

|       | Low pI | Medium pI | High pI |
|-------|--------|-----------|---------|
| $L_1$ | 41.3%  | 47.0%     | 11.7%   |
| $L_2$ | 42.1%  | 49.1%     | 8.8%    |
| $L_3$ | 50.2%  | 45.9%     | 3.9%    |

Similarly to the pI, we evaluated the molecular weight (MW) distributions of the investigated coronas. As Figure 3 clearly shows, adsorbed proteins had MW ranging from a few to a few hundred kDa and the largest portion of the distributions were found within about 40 kDa and 100 kDa, independently on lipid formulations and protein sources. Further-

more, all the curves exhibited a remarkable peak at about 11 kDa and minor contributions within 15–40 kDa and 100–500 kDa. In the specular representations of Figure 3, vertical solid lines quantify the detected differences between healthy (CTR) and pancreatic cancer (PDAC) coronas. Horizontal lines indicate the dominant contributions to such differences, which were mainly due to the proteins listed on the right and in Table 3. In this regard, some clear trends can be outlined. As an instance, complement C4-A and C4-B (CO4A and CO4B, respectively, MW = 193 kDa) were found to be significantly downregulated in all the PDAC coronas, complement component 3 (CO3, MW = 187 kDa), C4b-binding protein (C4BPA, MW = 67 kDa) and platelet basic protein (CXCL7, MW = 14 kDa) were significantly downregulated in PDAC samples for two out of three liposome formulations. Among the upregulated proteins in PDAC samples, the most significant differences corresponded to fibrinogen gamma chain (FIBG, MW = 52 kDa), serum amyloid A-2 (SAA2, MW = 14 kDa) and apolipoprotein C-II (APOC2, MW = 11 kDa), which were detected with larger relative protein abundances (RPAs) for at least one of the three liposomes. Finally, some proteins exhibited opposite trends, e.g., fibrinogen alpha and beta chains (FIBA and FIBB, MW = 95 kDa and MW = 56 kDa, respectively) were more abundant in PDAC coronas for the cationic liposome and in CTR coronas for the neutral one. The same trend was detected for apolipoprotein C-III (APOC3, MW = 11 kDa), while apolipoprotein E (APOE, MW = 36 kDa) and apolipoprotein A-II (APOA2, 11 kDa) were more abundant in cancer coronas for the anionic liposome and less abundant for the cationic and neutral formulations, respectively.
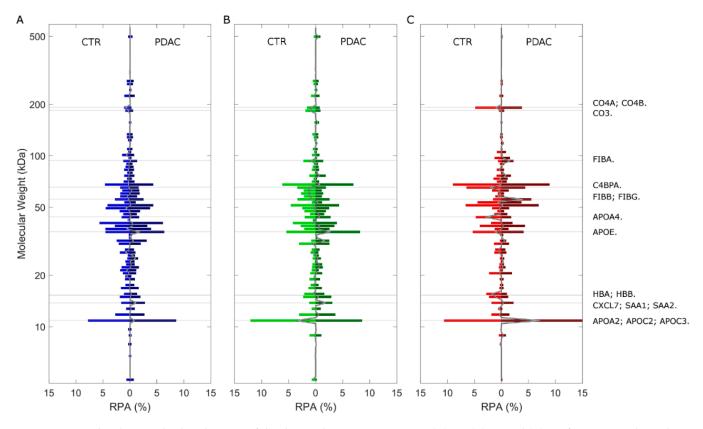


**Figure 3.** Molecular weight distributions of the detected corona proteins on (**A**) $L_1$, (**B**) $L_2$ and (**C**) $L_3$, for non-oncological (left) and PDAC (right) samples. Arithmetical differences between PDAC and CTR distributions are shown as solid vertical lines and proteins contributing most to such differences are listed on the right and located according to their molecular weight.

**Table 3.** Relative protein abundances (RPAs) of the most represented (RPA > 1%) proteins underlying the differences between PDAC and non-oncological coronas.

| Protein | MW (kDa) | pI | Relative Protein Abundance on Healthy Corona | | | Relative Protein Abundance on PDAC Corona | | | Difference | | |
|---|---|---|---|---|---|---|---|---|---|---|---|
| | | | L1 | L2 | L3 | L1 | L2 | L3 | L1 | L2 | L3 |
| CO4A | 193 | 7 | 0.48 ± 0.12% | 0.77 ± 0.06% | 2.42 ± 0.17% | 0.00 ± 0.00% | 0.32 ± 0.04% | 1.86 ± 0.20% | − | − | − |
| CO4B | 193 | 7 | 0.55 ± 0.03% | 0.81 ± 0.06% | 2.45 ± 0.15% | 0.26 ± 0.04% | 0.42 ± 0.05% | 1.92 ± 0.20% | − | − | − |
| CO3 | 187 | 6 | 0.69 ± 0.05% | 1.75 ± 0.23% | 0.45 ± 0.07% | 0.42 ± 0.03% | 0.77 ± 0.07% | 0.46 ± 0.06% | − | − | |
| FIBA | 95 | 6 | 1.18 ± 0.26% | 2.10 ± 0.35% | 0.66 ± 0.12% | 1.26 ± 0.53% | 1.30 ± 0.30% | 2.22 ± 0.77% | | − | + |
| C4BPA | 67 | 7 | 0.42 ± 0.09% | 1.04 ± 0.27% | 5.43 ± 0.62% | 0.35 ± 0.10% | 0.50 ± 0.09% | 3.62 ± 0.66% | | − | − |
| FIBB | 56 | 8 | 1.92 ± 0.27% | 2.81 ± 0.02% | 1.28 ± 0.20% | 1.98 ± 0.63% | 2.18 ± 0.46% | 5.12 ± 1.07% | | − | + |
| FIBG | 52 | 5 | 1.48 ± 0.10% | 1.88 ± 0.11% | 0.77 ± 0.06% | 1.63 ± 0.65% | 1.49 ± 0.36% | 2.25 ± 0.64% | | | + |
| APOA4 | 45 | 5 | 0.62 ± 0.08% | 1.00 ± 0.16% | 3.88 ± 0.86% | 0.41 ± 0.20% | 0.60 ± 0.29% | 0.99 ± 0.08% | | | − |
| APOE | 36 | 5 | 0.78 ± 0.05% | 2.11 ± 0.17% | 2.44 ± 0.41% | 1.29 ± 0.29% | 2.16 ± 0.51% | 1.37 ± 0.06% | + | | − |
| HBB | 16 | 7 | 0.80 ± 0.11% | 1.43 ± 0.19% | 1.57 ± 1.88% | 0.98 ± 0.35% | 1.18 ± 0.40% | 0.42 ± 0.08% | | | |
| HBA | 15 | 9 | 0.82 ± 0.12% | 1.11 ± 0.21% | 1.48 ± 1.68% | 0.71 ± 0.31% | 1.12 ± 0.48% | 0.35 ± 0.04% | | | |
| CXCL7 | 14 | 9 | 0.76 ± 0.12% | 0.52 ± 0.06% | 0.74 ± 0.44% | 0.45 ± 0.04% | 0.13 ± 0.12% | 0.27 ± 0.20% | − | − | |
| SAA1 | 14 | 7 | 0.00 ± 0.00% | 0.03 ± 0.05% | 0.66 ± 0.07% | 0.04 ± 0.07% | 0.71 ± 0.93% | 0.91 ± 0.36% | | | |
| SAA2 | 14 | 10 | 0.00 ± 0.00% | 0.00 ± 0.00% | 1.33 ± 1.32% | 0.40 ± 0.45% | 0.31 ± 0.14% | 0.92 ± 0.61% | | + | |
| APOA2 | 11 | 7 | 0.83 ± 0.16% | 2.21 ± 0.47% | 1.51 ± 0.31% | 1.48 ± 0.47% | 1.23 ± 0.14% | 1.35 ± 0.08% | + | − | |
| APOC2 | 11 | 4 | 1.02 ± 0.07% | 1.49 ± 0.30% | 2.19 ± 0.34% | 1.45 ± 0.34% | 1.17 ± 0.03% | 4.14 ± 1.26% | + | | + |
| APOC3 | 11 | 5 | 2.33 ± 0.25% | 4.03 ± 0.87% | 3.94 ± 0.49% | 1.78 ± 0.74% | 2.30 ± 0.71% | 10.5 ± 2.15% | | − | + |

We incidentally state that all those differences are simply evaluated by arithmetical subtraction of the detected RPAs on PDAC and CTR samples, protein by protein. Thus, the aforementioned dominant contributions are intrinsically related to corona proteins that were quite abundant (RPA $\geq$ 1%) in at least one of the investigated samples. To take into account the statistical significance between non-oncological and PDAC coronas, we studied the PDAC-to-healthy RPA ratio and the corresponding *p*-value from Student's *t*-test, for each of the detected proteins. Results are shown in Figure 4 as Volcano plots. Dots located in the upper region of the graphs correspond to upregulated proteins in the corona of the specific liposomal dispersion. Similarly, dots located in the lower region correspond to downregulated corona proteins. For each point, the x-location represents the *p*-value from *t*-test, which was evaluated by comparing the non-oncological and PDAC RPA. For each liposome, proteins with $|\log_2 (\text{fold change})| > 1$ and $p < 0.01$ were identified as the most significant and their (abbreviated) names are reported in each panel. This analysis provides a way to find even small, but significant differences between the RPAs of single proteins, separately for each of the three liposomal formulations.

To detect common trends along all the explored liposomal formulation, and thus to take into account proteins with small abundance in the coronas, but that may be expressed differently in PDAC and non-oncological patients, we employed a different approach. For each of the detected proteins, we defined an RPA-based parameter as

$$\lambda^i{}_j = \frac{x^i{}_j - y^i{}_j}{x^i{}_j + y^i{}_j} \qquad (1)$$

where $x^i{}_j$ and $y^i{}_j$ are the RPA of the *i*-th protein in the PDAC and CTR coronas, respectively, on the *j*-th formulation (*j* = 1, 2, 3). It can be easily demonstrated that $-1 \leq \lambda \leq 1$, where $\lambda = -1$ if $x = 0$ and $y > 0$ (i.e., the generic protein populates the CTR corona but not the PDAC ones) and $\lambda = 1$ if $y = 0$ and $x > 0$ (i.e., the generic protein populates the PDAC corona but not the CTR ones). In other words, $\lambda$ is a normalized parameter that quantifies the unbalance of the protein abundance towards the healthy (negative values) or the PDAC condition (positive values). If $\lambda$ is close to zero, then the measured RPA of that protein is almost the same in CTR and PDAC coronas. As we used three formulations, we associated a set of three coordinates $(\lambda_1; \lambda_2; \lambda_3)$ to each protein and represented the corresponding data points in a three-dimensional space. Thus, data points are scattered in a cubic box, as shown in Figure 5. Proteins located near the center populate almost

equally healthy and cancer coronas for all three liposomes. Conversely, proteins with larger RPAs in the PDAC coronas than the CTR ones are in the top right corner, since their $\lambda$-values tend to reach the maximum for all the liposomal formulations. Similarly, proteins with lower RPAs in the PDAC coronas than the CTR ones are located near the bottom left corner. A list of these most representative proteins is provided in Table 4. These proteins exhibit remarkable differences of relative abundances between cancer and non-oncological coronas, simultaneously on all the investigated liposomal formulations. Thus, the measured differences are most likely due to upregulation or downregulation of the protein expressions that are triggered by the pathological condition and are detected by the employment of NPs as "nano-accumulators". Indeed, the average abundance of those proteins is quite small (RPA $\leq$ 1%), but the aforementioned approach allowed us to distinguish the most relevant small but significant variations between PDAC and CTR samples. As an instance, ficolin-3 (FCN3) and carboxypeptidase N catalytic chain (CBPN) are almost absent on all the CTR coronas but populate all the PDAC counterparts, yielding to significant variations of the measured RPAs (i.e., the $p$-values from Student's test are 0.041, 0.006 and 0.001 for FCN3 on $L_1$, $L_2$ and $L_3$ and 0.009, 0.002, and 0.0001 for CBPN on $L_1$, $L_2$ and $L_3$, respectively). Proteins exhibiting opposite trends are located within the other box's corner, e.g., histidine-rich glycoprotein (HRG, $p$-values equal to $8.5 \times 10^{-6}$, 0.011 and 0.063 for $L_1$, $L_2$ and $L_3$, respectively).
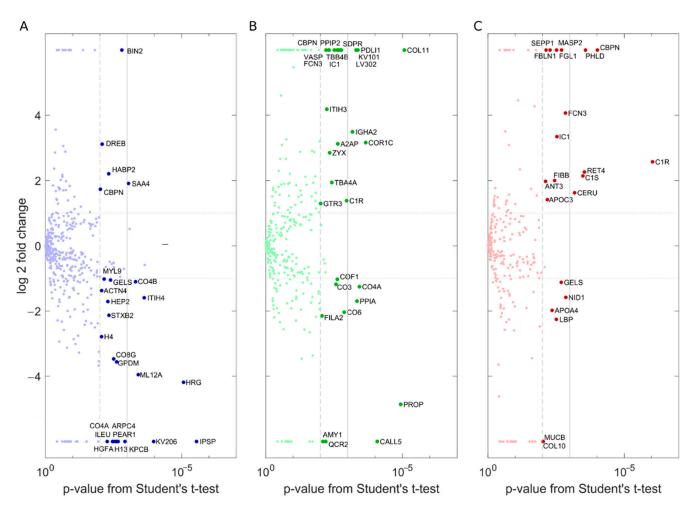


**Figure 4.** Volcano plots depicting corona proteins, whose RPAs are significantly different between healthy and PDAC samples, in terms of fold-changes and $p$-values from Student's $t$-test, for (**A**) $L_1$, (**B**) $L_2$ and (**C**) $L_3$.
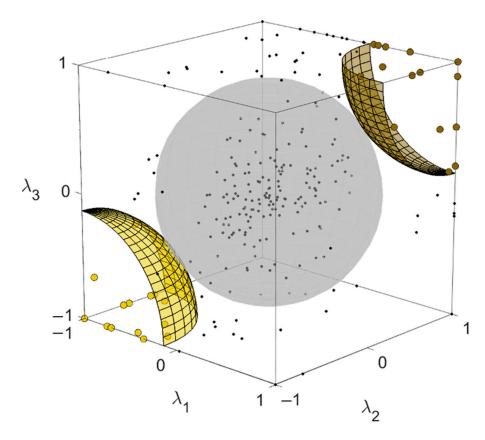
**Figure 5.** Scatter plot of the λ–values for L1, L2, and L3, as defined in Equation (1). Each protein is represented as a dot in the cubic box. Proteins located near the center populate almost equally healthy and cancer coronas for all the three liposomes. Conversely, proteins with larger RPAs in the PDAC coronas than the CTR ones are located in the top right corner and proteins with smaller RPAs in the PDAC coronas than the CTR ones are located in the bottom left corner.

**Table 4.** Relative abundances of proteins which exhibited major differences between healthy and PDAC coronas, simultaneously for all the employed formulations.

| Protein | MW (kDa) | pI | RPA on Healthy Corona | | | RPA on PDAC Corona | | |
|---|---|---|---|---|---|---|---|---|
| | | | L1 | L2 | L3 | L1 | L2 | L3 |
| FCN3 | 33 | 6.7 | 0.00 ± 0.00% | 0.00 ± 0.00% | 0.03 ± 0.03% | 1.50 ± 0.88% | 1.72 ± 0.57% | 0.54 ± 0.10% |
| CBPN | 52 | 7.4 | 0.05 ± 0.02% | 0.00 ± 0.00% | 0.00 ± 0.00% | 0.19 ± 0.04% | 0.11 ± 0.02% | 0.07 ± 0.02% |
| IC1 | 55 | 6.5 | 0.02 ± 0.01% | 0.00 ± 0.00% | 0.02 ± 0.02% | 0.07 ± 0.05% | 0.18 ± 0.04% | 0.22 ± 0.05% |
| CNN2 | 34 | 7.4 | 0.12 ± 0.03% | 0.00 ± 0.00% | 0.00 ± 0.00% | 0.22 ± 0.02% | 0.11 ± 0.07% | 0.09 ± 0.15% |
| VASP | 40 | 9.4 | 0.20 ± 0.07% | 0.00 ± 0.00% | 0.00 ± 0.01% | 0.35 ± 0.04% | 0.18 ± 0.04% | 0.07 ± 0.07% |
| IGHA2 | 37 | 6 | 0.08 ± 0.13% | 0.08 ± 0.14% | 0.05 ± 0.08% | 0.26 ± 0.16% | 0.91 ± 0.06% | 0.12 ± 0.20% |
| CALD1 | 93 | 5.4 | 0.05 ± 0.02% | 0.00 ± 0.00% | 0.00 ± 0.00% | 0.08 ± 0.01% | 0.06 ± 0.03% | 0.01 ± 0.01% |
| MASP1 | 79 | 5.2 | 0.00 ± 0.00% | 0.00 ± 0.00% | 0.16 ± 0.04% | 0.02 ± 0.02% | 0.03 ± 0.03% | 0.23 ± 0.02% |
| CALL5 | 16 | 4.1 | 0.02 ± 0.03% | 0.21 ± 0.02% | 0.14 ± 0.19% | 0.00 ± 0.00% | 0.00 ± 0.00% | 0.00 ± 0.00% |
| H4 | 11 | 11.9 | 0.24 ± 0.04% | 0.16 ± 0.28% | 0.07 ± 0.12% | 0.03 ± 0.06% | 0.00 ± 0.00% | 0.00 ± 0.00% |
| QCR2 | 48 | 8.9 | 0.08 ± 0.03% | 0.04 ± 0.01% | 0.01 ± 0.01% | 0.01 ± 0.01% | 0.00 ± 0.00% | 0.00 ± 0.00% |
| ML12A | 20 | 4.4 | 0.34 ± 0.03% | 0.11 ± 0.15% | 0.05 ± 0.06% | 6.00 ± 0.03% | 0.00 ± 0.00% | 0.01 ± 0.02% |
| MUCB | 43 | 4.9 | 0.22 ± 0.19% | 0.51 ± 0.89% | 0.25 ± 0.09% | 0.00 ± 0.00% | 0.13 ± 0.23% | 0.00 ± 0.00% |
| PROP | 51 | 7.9 | 0.12 ± 0.01% | 0.67 ± 0.04% | 0.03 ± 0.02% | 0.04 ± 0.03% | 0.02 ± 0.02% | 0.00 ± 0.00% |
| CO8G | 22 | 8.5 | 0.15 ± 0.03% | 0.28 ± 0.12% | 0.04 ± 0.04% | 0.01 ± 0.02% | 0.15 ± 0.04% | 0.00 ± 0.00% |
| HRG | 60 | 7.5 | 0.37 ± 0.01% | 0.41 ± 0.09% | 0.13 ± 0.04% | 0.02 ± 0.02% | 0.12 ± 0.07% | 0.06 ± 0.02% |

## 4. Discussion

In this work, we studied the protein corona that forms on anionic, neutral, and cationic liposomes upon exposure to human plasma from non-oncological donors and pancreatic ductal adenocarcinoma (PDAC) patients. A physical-chemical characterization of these systems confirmed some known effects of protein adsorption on nanoparticles, i.e., a remarkable size increase and the "normalization" of the zeta potential to negative values, independently on the original surface charge of the pristine objects. Unfortunately and expectedly, the study of these trends did not provide valuable information for diagnostic applications, e.g., to distinguish healthy and PDAC samples. Thus, an evaluation of the protein corona composition was needed and was performed by mass spectrometry experiments. Global differences among the coronas of anionic, neutral and cationic liposomes were found. As an instance, proteins with a low isoelectric point (pI) tend to populate more the corona of anionic liposomes, whereas high-pI proteins were more abundant for cationic liposomes. This behavior is more likely due to the electrostatic interactions between the nanoplatforms and the surrounding biomolecules. Despite the electrostatic force is not the unique contribution to the formation of the protein corona, our results clearly indicate that it has a significant role in shaping the corona composition. To find specific differences between healthy PDAC samples, we adopted different approaches. The study of the molecular weight distribution and the fold-change coupling with *p*-values provided information about the most abundant discriminating proteins and the most statistically significant contributions, respectively. These analyses are focused on the specific corona of each single liposome. On the other hand, the evaluation of a global parameter (i.e., λ, Equation (1)) that takes into account general trends for all the investigated systems, allowed us to identify potential biomarkers for PDAC.

Globally, our results are consistent with what already reported in the literature. Complement elements and their binding proteins have been already described as associated with pancreatic cancer [15,18]. Moreover, Chen conducting a quantitative proteomics analysis of rats pancreatic rough endoplasmic reticulum found a dramatic increase in fibrinogen alpha, beta and gamma chains in presence of acute pancreatitis [19].

As for SAA2, in our experience, it was found abundant in the corona of PDAC subjects. In this regard, it should be noted that Lee, studying the predisposition of the liver to act as a niche for cancer cells, reported how during pancreatic tumorigenesis in mice, hepatocytes activate molecular signaling that increase the production of SAA. Moreover, higher circulating levels of SAA have also been detected in liver metastatic PDAC and colorectal patients [20].

Nonetheless, previous experiences of proteomics analysis performed on serum of PDAC patients lead to identify in apolipoprotein CII and CIII potential biomarkers of this lethal disease. Furthermore, since ApoCII has been found able to significantly increase both tumor growth and invasion, it has been proposed as selector of patients for pancreaticoduodenectomy [21].

To the best of our knowledge, so far less has been reported about the role of Ficolin-3 in pancreatic cancer. Since it has been found significantly increased in other GI tract tumors [22] we can speculate an important role of this lectin pathway molecule that may participate in the host immune response against cancer, even in PDAC.

## 5. Conclusions

Current efforts aim to develop new technologies for the early detection of PDAC, a very lethal malignancy, already recognized as one of the biggest cancer killers in wealthy countries and for which there are currently no sensitive and specific biomarkers. In this work, we applied MS/MS to identify plasma proteins that enrich the protein corona of anionic, neutral, and cationic liposomes upon exposure to human plasma from non-oncological donors and PDAC patients. Corona proteins were ranked for their ability to discriminate PDAC patients from healthy subjects. While some discriminating proteins are already accepted as PDAC biomarkers, some others (e.g., Ficolin-3) do not have a

clear role in PDAC onset and progression. Therefore, we envision that characterization of the liposome-protein corona may pave the way for the discovery of new sensitive PDAC biomarkers and may contribute to increase our knowledge of PDAC biology.

**Author Contributions:** Conceptualization, D.P., D.C. and G.C.; Data curation, L.D.; Formal analysis, L.D.; Investigation, L.D., F.G., A.C. and V.L.V.; Methodology, L.D.; Project administration, D.P., D.C. and G.C.; Resources, D.P. and G.C.; Software, L.D.; Supervision, G.C.; Validation, F.G., A.C. and V.L.V.; Writing—review & editing, D.P., D.C. and G.C. All authors have read and agreed to the published version of the manuscript.

**Institutional Review Board Statement:** The study was conducted according to the guidelines of the Declaration of Helsinki, and approved by the Ethics Committee of University Campus Bio-Medico di Roma (Prot.: 10.4(12).21 OSS).

**Informed Consent Statement:** Informed consent was obtained from all subjects involved in the study.

**Data Availability Statement:** The data that support the findings of this study are available from the corresponding author upon reasonable request.

**Conflicts of Interest:** The authors declare no conflict of interest.

## References

1.  Caputo, D.; Caracciolo, G. Nanoparticle-enabled blood tests for early detection of pancreatic ductal adenocarcinoma. *Cancer Lett.* **2020**, *470*, 191–196. [CrossRef]
2.  Digiacomo, L.; Cardarelli, F.; Pozzi, D.; Palchetti, S.; Digman, M.A.; Gratton, E.; Capriotti, A.L.; Mahmoudi, M.; Caracciolo, G. An apolipoprotein-enriched biomolecular corona switches the cellular uptake mechanism and trafficking pathway of lipid nanoparticles. *Nanoscale* **2017**, *9*, 17254–17262. [CrossRef] [PubMed]
3.  Walkey, C.D.; Chan, W.C.W. Understanding and controlling the interaction of nanomaterials with proteins in a physiological environment. *Chem. Soc. Rev.* **2012**, *41*, 2780–2799. [CrossRef]
4.  Tenzer, S.; Docter, D.; Kuharev, J.; Musyanovych, A.; Fetz, V.; Hecht, R.; Schlenk, F.; Fischer, D.; Kiouptsi, K.; Reinhardt, C.; et al. Rapid formation of plasma protein corona critically affects nanoparticle pathophysiology. *Nat. Nanotechnol.* **2013**, *8*, 772–781. [CrossRef] [PubMed]
5.  Monopoli, M.P.; Åberg, C.; Salvati, A.; Dawson, K.A. Biomolecular coronas provide the biological identity of nanosized materials. *Nat. Nanotechnol.* **2012**, *7*, 779–786. [CrossRef] [PubMed]
6.  Corbo, C.; Molinaro, R.; Tabatabaei, M.; Farokhzad, O.C.; Mahmoudi, M. Personalized protein corona on nanoparticles and its clinical implications. *Biomater. Sci.* **2017**, *5*, 378–387. [CrossRef] [PubMed]
7.  Caracciolo, G.; Safavi-Sohi, R.; Malekzadeh, R.; Poustchi, H.; Vasighi, M.; Chiozzi, R.Z.; Capriotti, A.L.; Laganà, A.; Hajipour, M.; Di Domenico, M.; et al. Disease-specific protein corona sensor arrays may have disease detection capacity. *Nanoscale Horiz.* **2019**, *4*, 1063–1076. [CrossRef]
8.  Di Santo, R.; Digiacomo, L.; Quagliarini, E.; Capriotti, A.L.; Laganà, A.; Chiozzi, R.Z.; Caputo, D.; Cascone, C.; Coppola, R.; Pozzi, D.; et al. Personalized graphene oxide-protein corona in the human plasma of pancreatic cancer patients. *Front. Bioeng. Biotechnol.* **2020**, *8*, 491. [CrossRef]
9.  Papafilippou, L.; Claxton, A.; Dark, P.; Kostarelos, K.; Hadjidemetriou, M. Protein corona fingerprinting to differentiate sepsis from non-infectious systemic inflammation. *Nanoscale* **2020**, *12*, 10240–10253. [CrossRef]
10. Hadjidemetriou, M.; Rivers-Auty, J.; Papafilippou, L.; Eales, J.; Kellett, K.A.B.; Hooper, N.M.; Lawrence, C.B.; Kostarelos, K. Nanoparticle-enabled enrichment of longitudinal blood proteomic fingerprints in Alzheimer's disease. *ACS Nano* **2021**, *15*, 7357–7369. [CrossRef]
11. Hadjidemetriou, M.; Papafilippou, L.; Unwin, R.D.; Rogan, J.; Clamp, A.; Kostarelos, K. Nano-scavengers for blood biomarker discovery in ovarian carcinoma. *Nano Today* **2020**, *34*, 100901. [CrossRef]
12. Caputo, D.; Papi, M.; Coppola, R.; Palchetti, S.; Digiacomo, L.; Caracciolo, G.; Pozzi, D. A protein corona-enabled blood test for early cancer detection. *Nanoscale* **2016**, *9*, 349–354. [CrossRef] [PubMed]
13. Yeo, T.P.; Hruban, R.H.; Leach, S.D.; Wilentz, R.E.; Sohn, T.A.; Kern, S.E.; Iacobuzio-Donahue, C.A.; Maitra, A.; Goggins, M.; Canto, M.I.; et al. Pancreatic cancer. *Curr. Probl. Cancer* **2002**, *26*, 176–275. [CrossRef] [PubMed]
14. Papi, M.; Palmieri, V.; Digiacomo, L.; Giulimondi, F.; Palchetti, S.; Ciasca, G.; Perini, G.; Caputo, D.; Cartillone, M.C.; Cascone, C.; et al. Converting the personalized biomolecular corona of graphene oxide nanoflakes into a high-throughput diagnostic test for early cancer detection. *Nanoscale* **2019**, *11*, 15339–15346. [CrossRef] [PubMed]

15. Caputo, D.; Cartillone, M.; Cascone, C.; Pozzi, D.; Digiacomo, L.; Palchetti, S.; Caracciolo, G.; Coppola, R. Improving the accuracy of pancreatic cancer clinical staging by exploitation of nanoparticle-blood interactions: A pilot study. *Pancreatology* **2018**, *18*, 661–665. [CrossRef] [PubMed]

16. Caracciolo, G.; Pozzi, D.; Capriotti, A.L.; Cavaliere, C.; Piovesana, S.; Amenitsch, H.; Lagana, A. Lipid composition: A "key factor" for the rational manipulation of the liposome–protein corona by liposome design. *RSC Adv.* **2015**, *5*, 5967–5975. [CrossRef]

17. Digiacomo, L.; Giulimondi, F.; Capriotti, A.L.; Piovesana, S.; Montone, C.M.; Chiozzi, R.Z.; Laganà, A.; Mahmoudi, M.; Pozzi, D.; Caracciolo, G. Optimal centrifugal isolating of liposome–protein complexes from human plasma. *Nanoscale Adv.* **2021**. [CrossRef]

18. Sogawa, K.; Yamanaka, S.; Takano, S.; Sasaki, K.; Miyahara, Y.; Furukawa, K.; Takayashiki, T.; Kuboki, S.; Takizawa, H.; Nomura, F.; et al. Fucosylated C4b-binding protein α-chain, a novel serum biomarker that predicts lymph node metastasis in pancreatic ductal adenocarcinoma. *Oncol. Lett.* **2020**, *21*, 1. [CrossRef]

19. Chen, X.; Sans, M.D.; Strahler, J.R.; Karnovsky, A.; Ernst, S.A.; Michailidis, G.; Andrews, P.C.; Williams, J.A. Quantitative organellar proteomics analysis of rough endoplasmic reticulum from normal and acute pancreatitis rat pancreas. *J. Proteome Res.* **2010**, *9*, 885–896. [CrossRef]

20. Lee, J.W.; Stone, M.L.; Porrett, P.M.; Thomas, S.; Komar, C.A.; Li, J.H.; Delman, D.; Graham, K.; Gladney, W.L.; Hua, X.; et al. Hepatocytes direct the formation of a pro-metastatic niche in the liver. *Nat. Cell Biol.* **2019**, *567*, 249–252. [CrossRef]

21. Xue, A.; Chang, J.W.; Chung, L.; Samra, J.; Hugh, T.; Gill, A.; Butturini, G.; Baxter, R.C.; Smith, R.C. Serum apolipoprotein C-II is prognostic for survival after pancreatic resection for adenocarcinoma. *Br. J. Cancer* **2012**, *107*, 1883–1891. [CrossRef] [PubMed]

22. Li, Q.; Lin, Y. Evaluation of Ficolin-3 as a Potential Prognostic Serum Biomarker in Chinese Patients with Esophageal Cancer. *Genet. Test. Mol. Biomark.* **2019**, *23*, 565–572. [CrossRef] [PubMed]